

## Magnetic transition and magnetocaloric effect in $\text{La}_{1-x}\text{Ca}_x\text{MnO}_3$ compounds

M. S. Anwar, Shalendra Kumar, Faheem Ahmed, Sung Chang Hoon, Si Nae Heo and Bon Heun Koo\*

School of Nano and Advanced Materials Engineering, Changwon National University, Changwon, Gyeongnam 641-773, Korea

We report the magnetic transition and large magnetic entropy change in calcium doped lanthanum manganites. Polycrystalline  $\text{La}_{1-x}\text{Ca}_x\text{MnO}_3$  ( $0 \leq x \leq 0.4$ ) samples were prepared by the conventional solid-state reaction technique. The X-ray diffraction analysis exhibits only the perovskite phase without any impurity. It was found that the Curie temperature is varied with the Ca-concentration because of the doping of Ca at La site affects the Mn-O bond length and Mn-O-Mn bond angle due to the difference in their ionic radii. A large magnetic entropy change was observed in the  $\text{La}_{0.7}\text{Ca}_{0.3}\text{MnO}_3$  sample and the value of the maximum entropy change ( $|\Delta S_M^{\max}|$ ), increase from 4.67 to 10.78 J/kgK as magnetic field increases from 1 to 5 tesla. This result suggests that  $\text{La}_{0.7}\text{Ca}_{0.3}\text{MnO}_3$  can be used as a potential magnetic refrigeration material.

**Key words:** Magnetic refrigeration, Magnetocaloric effect, Entropy, Manganites.

### Introduction

Recently, increasing attention has been paid to find the magnetic refrigerants with large magnetocaloric effect (MCE) near room temperature. The MCE is the tendency of certain materials, such as paramagnetic salts or ferromagnetic substances, to heat up when placed in a magnetic field and to cool down when removed from the field [1-3]. Among the magnetic materials with potential for magnetic refrigeration, the perovskite-type rare-earth manganites have attracted much attention due to their higher resistivity, which is favorable for reducing eddy current heating [4-9]. These compounds present also a relatively large magnetic entropy change [8, 9]. However, a large magnetic entropy change need a large magnetic field (up to several tesla), which limits its application. Therefore, many researchers intend to decrease the required magnetic field and much effort had been made to understand the physical properties of manganites.

High magnetic entropy change at low magnetic field changes and the broad working temperature ranges (due to easy controlling of the Curie temperature by doping routes) make these materials (manganites) good candidates as working elements in magnetic refrigeration applications [10, 11]. Moreover, low cost, ease of preparation, grain growth to a desired size via heat treatment, and high chemical stability are some other advantageous properties of these materials for use in magnetic refrigeration systems. Generally, the large magnetic entropy change of perovskite manganites mainly originates from the variation of the double

exchange (DE) interaction of the  $\text{Mn}^{3+}$  and  $\text{Mn}^{4+}$  ions [12]. In addition, the strong spin-lattice coupling also plays an important role [1, 13]. There are intensive studies on these materials which are reported in the literatures [14-16]. It is interesting to note that the samples with similar compositions shows different Curie temperature ( $T_c$ ) and magnetic entropy change values which appears to be due to varying preparation conditions. This is particularly evident in the case of  $\text{La}_{1-x}\text{Ca}_x\text{MnO}_3$  in which the Curie temperature varies in a broad temperature range of 170-280 K, indicating that it could be possible to optimize the magnetic properties by adjusting the preparation conditions.

This work aims to investigate the structural, magnetic properties and the magnetocaloric effects of  $\text{La}_{1-x}\text{Ca}_x\text{MnO}_3$  compounds in order to be helpful to understand the MCE of the magnetic refrigerant materials. The variation of structure and MCE were mainly studied as a function of Ca doping.

### Experimental procedure

Polycrystalline  $\text{La}_{1-x}\text{Ca}_x\text{MnO}_3$  ( $0 \leq x \leq 0.4$ ) samples were prepared by the conventional solid state reaction method. Appropriate ratio of  $\text{La}_2\text{O}_3$ , CaO and  $\text{Mn}_2\text{O}_3$  powders (all chemicals were 99.99% pure and purchased from Sigma Aldrich) were mixed according to the desired stoichiometry, and then calcined at 800 °C for 10 hour. The calcined powders were milled and then annealed at 1000 °C for 10 hours. Then the annealed mixture were milled again and pressed into a disk-shape with a diameter of 7 mm and a thickness of about 2 mm. The sintering process was performed at 1000 °C and 1250 °C for 24 hours in air. Finally, the furnace was cooled down to room temperature.

The crystal structure, phase purity, and cell dimensions

\*Corresponding author:  
Tel : +82-55-264-5431  
Fax: +82-55-262-6486  
E-mail: bhkoo@changwon.ac.kr

were determined using a X-ray diffractometer (XRD, Phillips X'pert (MPD 3040)) with Cu  $K\alpha$  radiations ( $\lambda = 1.5406 \text{ \AA}$ ) operated at voltage of 40 kV and current of 30 mA. Surface morphology was evaluated using a scanning electron microscope (SEM, JSM5610). Average grain size was determined by an intercept method using SEM micrographs. The magnetic measurements were carried out with a frequency of 40 Hz using a quantum design vibrating sample magnetometer PPMS-6000 ( $2 \leq T \leq 400 \text{ K}$ ,  $0 \leq H \leq 9 \text{ T}$ ) VSM.

## Results and discussion

The structural analysis of samples was performed using X-ray diffractometer with  $2\theta$  ranging from  $20^\circ$  to  $80^\circ$ . The XRD patterns of the sintered samples are given in Fig. 1. All the peaks reveal that the samples have single phase without any detectable secondary phase, indicating a complete reaction between reactants to form  $\text{La}_{1-x}\text{Ca}_x\text{MnO}_3$  samples. The characteristics reflections corresponding to (101), (121), (031), (220), (202), (212), (301), (311), (321), (424), (143) and (402) planes are indexed to an orthorhombic crystal structure using Powder-X software. The enlarged (121) peak (inset of Fig. 1) reveals that the peak shifts to lower angles with decreasing Ca doping concentration, indicating the change of lattice parameters. From the XRD patterns of the samples, the lattice parameters,  $c/a$  ratio and the unit cell volume were calculated and given in table 1. It was observed that lattice parameters ( $a$ ,  $b$  and  $c$ ) monotonically increases with decreasing Ca doping concentration. A similar behavior is also seen for the  $c/a$  ratio and unit cell volume. This is attributed to the change in A-site ionic radius  $\langle r_A \rangle$  [17].

Fig. 2 shows the SEM micrographs of  $\text{La}_{1-x}\text{Ca}_x\text{MnO}_3$  samples sintered at two different temperatures of  $1000^\circ\text{C}$  and  $1250^\circ\text{C}$ . It was observed that the samples sintered at  $1250^\circ\text{C}$  have mainly strongly connected

large grains as compared to the samples sintered at  $1000^\circ\text{C}$ . The average grain size was estimated to be  $\sim 7$ ,  $9$ , and  $9 \mu\text{m}$  for  $x = 0.4$ ,  $0.3$ , and  $0.2$ , respectively, for the samples sintered at  $1250^\circ\text{C}$ .

The field-cooled (FC) temperature dependence of the magnetization for  $\text{La}_{1-x}\text{Ca}_x\text{MnO}_3$  samples taken at 5000 Oe is shown in Fig. 3. In FC process, the sample was cooled from 305 K to 100 K under the applied magnetic field of 5000 Oe and then the magnetization measurement was performed under the same field

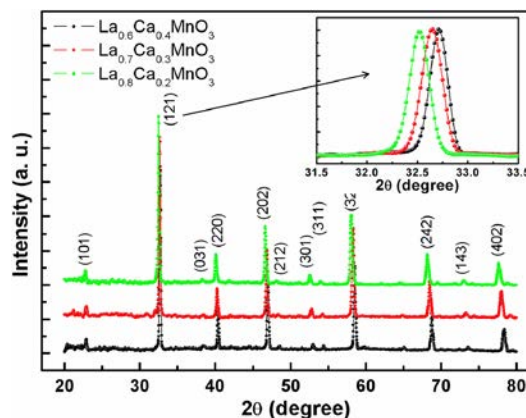


**Fig. 1.** X-ray diffraction patterns of  $\text{La}_{1-x}\text{Ca}_x\text{MnO}_3$ , ( $x = 0.4, 0.3$ , and  $0.2$ ) samples. The inset is the enlarged (121) peak in the diffraction patterns.

If you want that all figures printed in color, you need to pay the extra charge. Otherwise, you should revise all figures in B/W contrast, which can be seen correctly by the readers.

**Table 1.** Room temperature lattice parameters,  $c/a$  ratio and unit cell volumes of the samples.

X	a (Å)	b (Å)	c (Å)	c/a	V (Å <sup>3</sup> )
0.40	5.468	7.709	5.478	1.0018	230.91
0.30	5.490	7.758	5.503	1.0023	234.38
0.20	5.508	7.760	5.523	1.0027	236.06

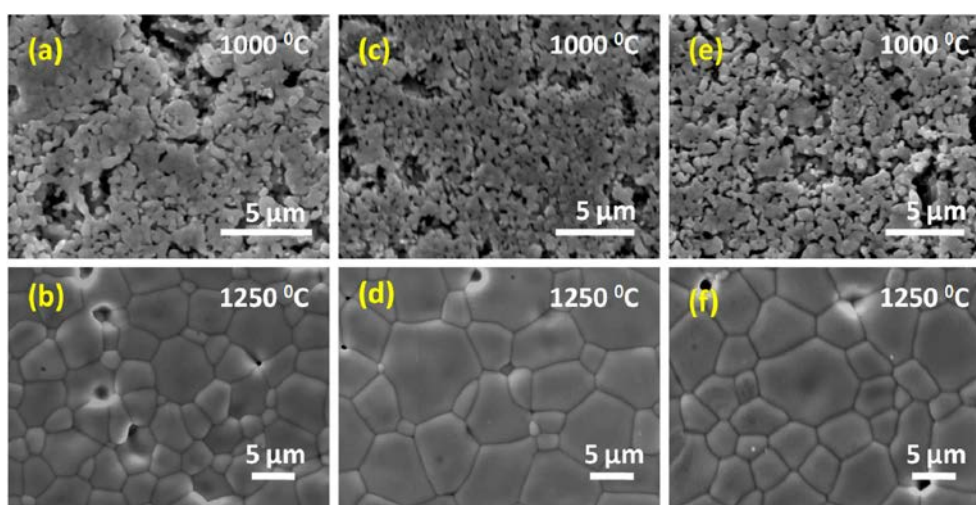


**Fig. 2.** SEM micrographs of the samples sintered at two different temperatures of  $1000^\circ\text{C}$  and  $1250^\circ\text{C}$  depending on the chemical composition: (a, b)  $\text{La}_{0.6}\text{Ca}_{0.4}\text{MnO}_3$ , (c, d)  $\text{La}_{0.7}\text{Ca}_{0.3}\text{MnO}_3$ , and (e, f)  $\text{La}_{0.8}\text{Ca}_{0.2}\text{MnO}_3$

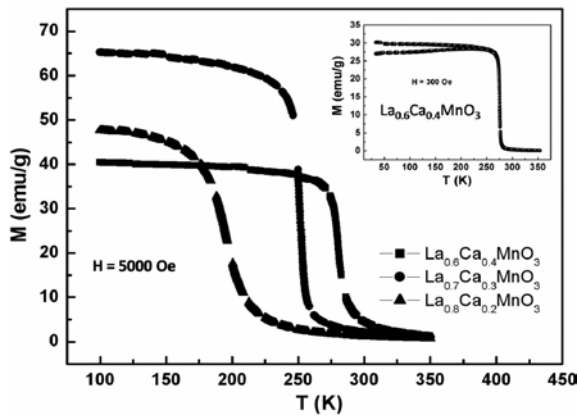


**Fig. 3.** Temperature dependence of the magnetization for the  $\text{La}_{1-x}\text{Ca}_x\text{MnO}_3$  ( $x = 0.4, 0.3$  and  $0.2$ ) samples. Inset indicated the ZFC and FC magnetizations for  $\text{La}_{0.6}\text{Ca}_{0.4}\text{MnO}_3$  under the applied magnetic field of 300 Oe.

If you want that all figures printed in color, you need to pay the extra charge. Otherwise, you should revise all figures in B/W contrast, which can be seen correctly by the readers.

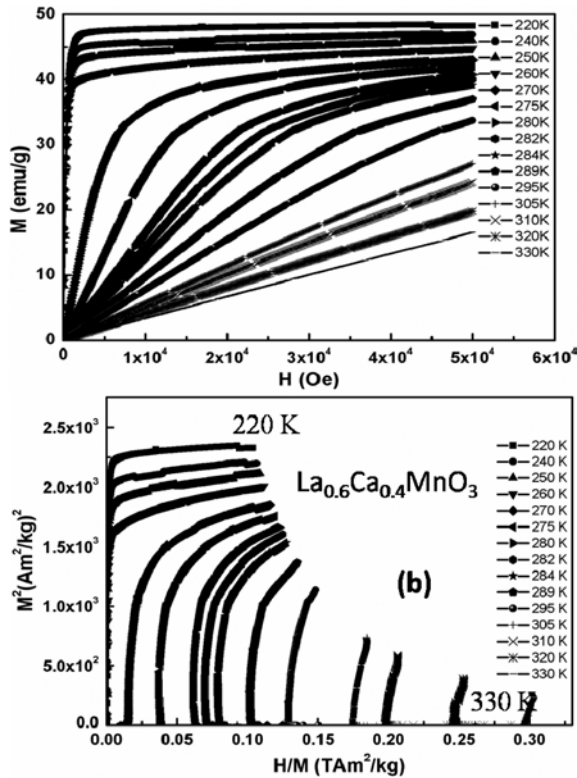


**Fig. 4.** (a) The field dependence of the magnetization measured at different temperatures around  $T_c$  and (b) Arrott plots for  $\text{La}_{0.6}\text{Ca}_{0.4}\text{MnO}_3$ .

If you want that all figures printed in color, you need to pay the extra charge. Otherwise, you should revise all figures in B/W contrast, which can be seen correctly by the readers.

during the warming up cycle from 100 K to 350 K. The variation of magnetization vs. temperature ( $M$ - $T$ ) reveals that the  $\text{La}_{1-x}\text{Ca}_x\text{MnO}_3$  samples exhibits a sharp ferromagnetic-paramagnetic (FM-PM) transition occurring at  $T_c$ . The Curie temperature, defined by the maximum in the absolute value of  $dM/dT$ , was found to be 278,

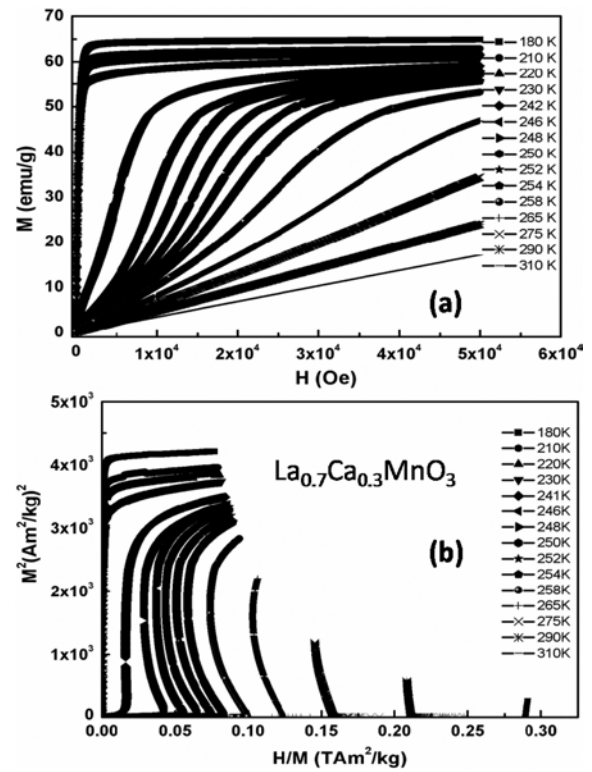


**Fig. 5.** (a) The field dependence of the magnetization measured at different temperatures around  $T_c$  and (b) Arrott plots for  $\text{La}_{0.7}\text{Ca}_{0.3}\text{MnO}_3$ .

If you want that all figures printed in color, you need to pay the extra charge. Otherwise, you should revise all figures in B/W contrast, which can be seen correctly by the readers.

250 and 198 K for  $x = 0.4, 0.3$  and  $0.2$ , respectively. Obviously, the  $T_c$  decreases monotonically with decreasing Ca-doping level. The change in  $T_c$  of the perovskite manganese oxides with an  $\text{ABO}_3$ -type structure is governed by two factors. One is the A-site average ionic radius  $\langle r_A \rangle$  and the other is the charge carrier density [18, 19]. It is suggested that the  $T_c$  reduction could be attributed to the combined effect of the partial destruction of  $\text{Mn}^{2+}$ -O- $\text{Mn}^{3+}$  DE interaction network and the weakening of DE interaction caused by Ca-doping. Inset of Fig. 3 shows  $M$ - $T$  for  $\text{La}_{0.6}\text{Ca}_{0.4}\text{MnO}_3$  sample under ZFC (zero-field-cooled) and FC conditions for an applied field of 300 Oe. There is ZFC-FC splitting occurring close to  $T_c$ . In FM material it can be related to the intrinsic magnetic anisotropy and to domain wall pinning in the magnetically ordered state so that applying a field, or not an applying field, while the cooling process through  $T_c$  leads to the different spin configuration that give rise to the different net magnetizations. In order to understand deeply the type of magnetic transition, the magnetization measurements versus applied magnetic field ( $M$ - $H$ ) was carried out up to 5 tesla at several temperatures near  $T_c$ . Fig. 4(a) and Fig. 5(a) show the  $M$ - $H$  behaviors for the  $\text{La}_{0.6}\text{Ca}_{0.4}\text{MnO}_3$  and  $\text{La}_{0.7}\text{Ca}_{0.3}\text{MnO}_3$  samples, respectively. The magnetization

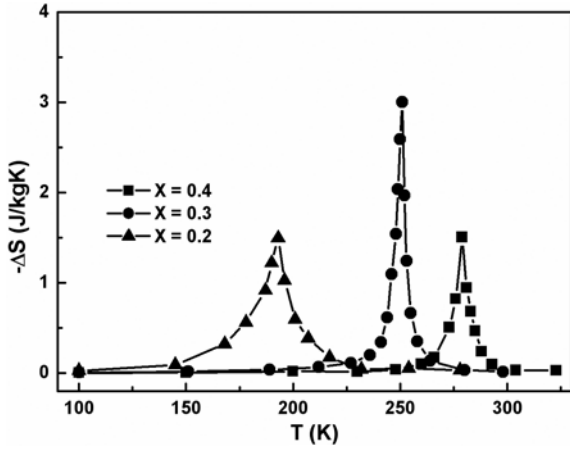


**Fig. 6.** Temperature dependence of magnetic entropy change at  $H = 0.5$  tesla for  $La_{1-x}Ca_xMnO_3$  ( $x = 0.4, 0.3$  and  $0.2$ ) samples.

If you want that all figures printed in color, you need to pay the extra charge. Otherwise, you should revise all figures in B/W contrast, which can be seen correctly by the readers.

below  $T_c$  sharply increases up to 0.5 tesla and then nearly gets saturated. We derive the Arrott plots ( $H/M$  vs.  $M^2$ ) from  $M$ - $H$  measurements and the results plotted as shown in Fig. 4(b) and Fig. 5(b).

A first order magnetic phase transition is particularly important for the giant MCE. The order of magnetic phase transition of the samples was confirmed by the Banerjee criterion [20]. The  $La_{0.7}Ca_{0.3}MnO_3$  sample shows the first order magnetic phase transition (FM to PM) behavior. However, the  $La_{0.6}Ca_{0.4}MnO_3$  sample reveals the mixed behavior of magnetic phase transition (first order and second order). As seen in Fig. 5(b),  $M^2$  does not show a linear relation but does have a convex curvature against  $H/M$  for most of isotherms. The convex curvature of  $M^2$  against  $H/M$  was also found in the MnSi specimen [21], which has typically a weak itinerant ferromagnetic property of the magnetization.

In order to evaluate the MCE, the total magnetic entropy change ( $\Delta S_M$ ) was calculated as a function of temperature and applied magnetic field. According to the thermodynamic theory based on Maxwell relations,  $\Delta S_M$  can be evaluated through the following equation; [22]

$$\Delta S_M(T, H) = S_M(T, H) - S_M(T, 0) = \int_0^H \left( \frac{\partial S}{\partial H} \right)_T dH \quad (1)$$

where  $H_{max}$  is the maximum value of the external applied magnetic field. In practice, for magnetization measurement, this relation can be approximated as follows;

$$-\Delta S_M(T, H) = \sum_i \frac{M_i - M_{i+1}}{T_{i+1} - T_i} \Delta H \quad (2)$$

where  $M_i$  and  $M_{i+1}$  are the experimental values of magnetization measured at temperatures  $T_i$  and  $T_{i+1}$ , respectively, under the applied magnetic field  $H_i$ .

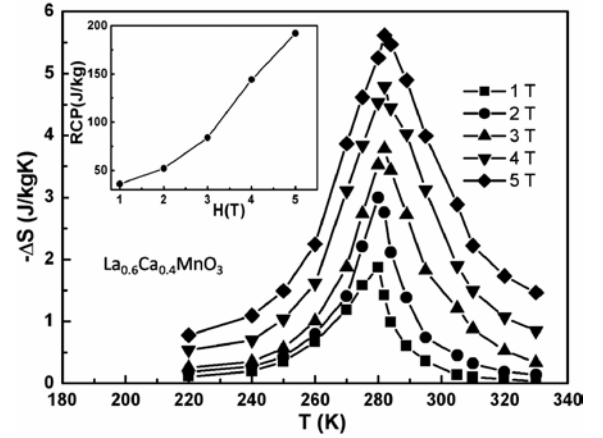


**Fig. 7.** Temperature dependence of magnetic entropy change under the different applied magnetic fields for  $La_{0.6}Ca_{0.4}MnO_3$  sample. The inset represents the RCP values vs. the applied magnetic field.

If you want that all figures printed in color, you need to pay the extra charge. Otherwise, you should revise all figures in B/W contrast, which can be seen correctly by the readers.

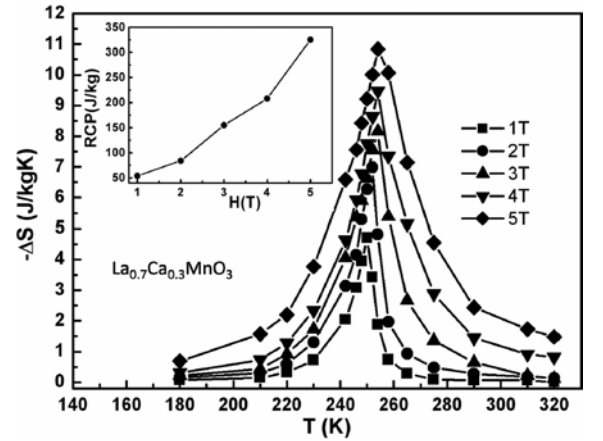


**Fig. 8.** Temperature dependence of magnetic entropy change under the different applied magnetic fields for  $La_{0.7}Ca_{0.3}MnO_3$  sample. The inset represents the RCP values vs. the applied magnetic field.

If you want that all figures printed in color, you need to pay the extra charge. Otherwise, you should revise all figures in B/W contrast, which can be seen correctly by the readers.

The evolution of  $|\Delta S_M^{max}|$  with Ca-doping variation is clearly seen in Fig. 6, exhibiting that the  $|\Delta S_M^{max}|$  first increases with decreasing Ca-doping and then decreased for  $x = 0.2$ . The abnormality on the maximum magnetic entropy change is observed. This different feature can be explained by the distorted crystal structure with the different composition ( $x$ ), which can cause the different change in the lattice parameters ( $a$ ,  $b$ , and  $c$ ) and bond angles with the variation of  $x$ , which influence  $\Delta S_M$  at  $T_c$ . The  $|\Delta S_M^{max}|$  values corresponding to a magnetic field variation of 0.5 tesla are found to be 1.51 J/kgK, 3.02 J/kgK, and 1.49 J/kgK for the  $La_{1-x}Ca_xMnO_3$  samples with  $x = 0.40, 0.30$ , and  $0.20$ , respectively.

Fig. 7 and Fig. 8 show the temperature dependence of the  $\Delta S_M$  under the different applied magnetic field for the  $La_{1-x}Ca_xMnO_3$  samples with  $x = 0.40$  and  $0.30$ , respectively. Both the samples exhibit a maximum

value in the magnetic entropy change,  $|\Delta S_M^{max}|$  in the vicinity of  $T_c$ , and increases with the applied magnetic field. In general, two parameters are necessary for inducing the large MCE. One is associated with a large enough spontaneous magnetization, while the other with an abrupt drop of the magnetization at  $T_c$ . Therefore, the samples exhibiting the second order magnetic phase transition are expected to show a reduced magnetic entropy change. The  $\text{La}_{0.7}\text{Ca}_{0.3}\text{MnO}_3$  sample shows the  $|\Delta S_M^{max}|$  of 6.94 J/kgK (Fig. 8) for  $H = 2$  tesla, which is much larger than that for Gd (4.2 J/kgK,  $H = 2$  tesla) [23]. On the other hand, the  $\text{La}_{0.6}\text{Ca}_{0.4}\text{MnO}_3$  sample shows the reduced  $|\Delta S_M^{max}|$  of 2.97 J/kgK for  $H = 2$  tesla, due to the mixed behavior of magnetic phase transition.

In the cooling applications, another important parameter is a relative cooling power (RCP), which is a good indicator of the cooling efficiency of a magnetic refrigerant. The RCP corresponds to the amount of heat transferred between the cold and the hot sinks in the refrigeration cycle and is defined as  $RCP(S) = -\Delta S_M^{max} \times \partial T_{FWHM}$ , where  $\partial T_{FWHM}$  is a full width at half maximum value of the temperature change. The RCP values for the  $\text{La}_{0.6}\text{Ca}_{0.4}\text{MnO}_3$  and  $\text{La}_{0.7}\text{Ca}_{0.3}\text{MnO}_3$  samples were calculated to be 52 J/kg and 85 J/kg, respectively for a field variation of 2 tesla. The RCP value increases with the applied magnetic field (inset of Fig. 7 and 8). On the other hand, the perovskite-type manganese oxides exhibit considerably small magnetic hysteresis with small coercivity of about 50 Oe near  $T_c$ , which would be beneficial for the magnetic cooling efficiency. Therefore, the  $\text{La}_{1-x}\text{Ca}_x\text{MnO}_3$  samples can be considered to be a good candidate for the magnetic refrigeration.

## Conclusions

The structural, magnetic and magnetocaloric properties of  $\text{La}_{1-x}\text{Ca}_x\text{MnO}_3$  with A-site doping have been investigated. The XRD results reveal that all the samples have an orthorhombic structure and the lattice parameters for  $\text{La}_{1-x}\text{Ca}_x\text{MnO}_3$  ( $0 \leq x \leq 0.4$ ) samples vary monotonically with decreasing Ca content. It is clearly shown that the ferromagnetic-paramagnetic transition temperature decreases with Ca doping, due to combined effect of the partial destruction of  $\text{Mn}^{2+}$ -O- $\text{Mn}^{3+}$  DE interaction network and the weakening of DE interaction. The Ca doping gives rise to a gradual crossover from a first- to second-order magnetic phase transition, resulting in the reduction of  $|\Delta S_M^{max}|$  with Ca doping. The experimental results suggest that these compounds can be used as the potential magnetic refrigerants with a wide range of working temperature.

## Acknowledgements

This research was supported by the National Research Foundation of Korea (NRF) grant funded by the Korea government (MEST) (No. 2011-0030802) and by the Ministry of Knowledge Economy (MKE) in Korea, under the ITRC (Information Technology Research Center) support program supervised by the NIPA (National IT Industry Promotion Agency) (NIPA-2012-H0301-12-2009).

## References

1. Z.B. Guo, Y.W. Du, J.S. Zhu, H. Huang, W.P. Ding, and D. Feng, Phys. Rev. Lett. 78 (1997) 1145.
2. R.N. Mahato, K. Sethupathi, V. Sankaranarayanan, R. Nirmala, J. Appl. Physics 107 (2010) 09A943.
3. Y. Regaiega, M. Koubaa, W. Cheikhrouhou Koubaa, A. Cheikhrouhou, T. Mhiri, J. Alloys Compd. 502 (2010) 270.
4. V.S. Kumar, R. Mahendiran, Solid State Commun. 150 (2010) 1445.
5. V.S. Kolat, H. Gencer, M. Gunes, S. Atalay, Mater. Sci. Eng. B 140 (2007) 212.
6. Z.B. Guo, Y.W. Du, J.S. Zhu, H. Huang, W.P. Ding, and D. Feng, Phys. Rev. Lett. 78 (1997) 1145.
7. M. Khelifi, M. Bejar, O.E. Sadek, E. Dhahri, M.A. Ahmed, E.K. Hlil, J. Alloys Compd. 509 (2011) 7410.
8. W.C. Koubaa, M. Koubaa, A. Cheikhrouhou, J. Alloys Compd. 509 (2011) 4363.
9. M. Oumezzine, S. Zemni, O. Pena, J. Alloys Compd. 508 (2010) 292.
10. M.H. Phan, S.C. Yu, J. Magn. Mater. 308 (2007) 325.
11. K.A. Gschneidner, V.K. Pecharsky, Int. J. Refrig. 31 (2008) 945.
12. M.H. Phan, S.C. Yu, N.H. Hur, J. Magn. Mater. 262 (2003) 407.
13. S.L. Yuan, Z.C. Xia, L. Liu, W. Chen, L.F. Zhao, J. Tang, G.H. Zhang, L.J. Zhang, H. Cao, W. Feng, Y. Tian, L. Y. Niu, S. Liu, Phys. Rev. B 68 (2003) 184423.
14. W.C.R. Koubaa, M. Koubaa, A. Cheikhrouhou, J. Alloys Compd. 470 (2009) 42.
15. J. Yang, W.H. Song, Y.Q. Ma, R.L. Zhang, B.C. Zhao, Z.G. Sheng, G.H. Zheng, J.M. Dai, Y.P. Sun, Phys. Rev. B 70 (2004) 092504.
16. C. Hao, B. Zhao, Y. Huang, G. Kuang, Y. Sun, J. Alloys Compd. 509 (2011) 5877.
17. Y. Samancioglu, A. Coskun, J. Alloys Compd. 507 (2010) 385.
18. Z.M. Wang, G. Ni, Q.Y. Xu, H. Sang, Y.W. Du, J. Appl. Phys. 90 (2001) 5689.
19. N. Kallel, S. Kallel, O. Pena, and M. Oumezzine, Solid State Sciences 11 (2009) 1494.
20. S.K. Banerjee, Phys. Lett. 12 (1964) 16.
21. D. Bloch, J. Voiron, V. Jaccarino, J.H. Wernick, Phys. Lett. 51A (1975) 259.
22. V.S. Kolat, T. Izgi, A.O. Kaya, N. Bayri, H. Gencer. S. Atalay, J. Magn. Mater. 322 (2010) 427.
23. Y. Dan'kov, A.M. Tishin, V.K. Pecharsky, K.A. Gschneidner Jr., Phys. Rev. B 57 (1998) 3478.